Bioorthogonal photocatalytic quinone methide decaging for cell-cell interaction labeling

Yan Zhang[2#], Shibo Liu[1#], Fuhu Guo[3], Shan Qin[2], Nan Zhou[1], Xinyuan Fan[1]* and Peng R. Chen[1,2]*

[1]Synthetic and Functional Biomolecules Center, Key Laboratory of Bioorganic Chemistry and Molecular Engineering of Ministry of Education, Beijing National Laboratory for Molecular Sciences, College of Chemistry and Molecular Engineering, Peking University, Beijing 100871, China.
[2]Peking-Tsinghua Center for Life Sciences, Peking University, Beijing 100871, China.
[3]College of Chemistry and Chemical Engineering, Northwest Normal University, Lanzhou, Gansu 730070, China.

Correspondence: pengchen@pku.edu.cn, xinyuanfan@pku.edu.cn

Abstract
Cell-cell interactions (CCIs) play crucial roles in directing diverse biological processes in multicellular organisms, making the high-sensitivity and selectivity characterization of the diverse CCIs in high demand yet still challenging. We herein introduced a bioorthogonal photocatalytic quinone methide decaging-enabled cell-cell interaction labeling strategy (CAT-Cell) for sensitive and spatiotemporally resolved profiling of multitype CCIs. By adapting an optimized quinone methide probe for interacting cell labeling, we demonstrated the excellent capacity of CAT-Cell for capturing and quantifying CCIs directed by various receptor-ligand pairs (e.g., CD40-CD40L, TCR-pMHC) and further showed its compatibility with tumor-specific targeting systems. Finally, we used CAT-Cell to detect cytotoxic cells (e.g., antigen-specific T cells, Natural Killer cells) in mouse models containing splenocyte mixtures and tumor samples. By leveraging the bioorthogonal photocatalytic decaging chemistry, CAT-Cell offers as a non-genetic, non-invasive and universal toolbox for profiling diverse CCIs under physiological-relevant settings.

Introduction
Direct cell-cell interactions are critical for diverse cellular activities, orchestrating essential biological processes such as embryonic development and homeostasis[1,2], highlighting the importance of decoding their interaction specificity under physiological as well as pathological conditions. The development of tumor is closely related to ubiquitous and complicated cellular interactions between cancer cells and tumor infiltrated immune cells co-existed in the tumor microenvironment (TME). Thus, it is crucial to investigate the heterogenous tumor infiltrated immune cell-tumor cell interactions in order to characterize immune responses and tumor progression, and to further guide immunotherapeutic applications[3-6]. Despite their importance, the highly dynamic nature, spatially restricted distance, as well as complex intercellular environment all made it highly challenging to capture the interacting cells. Furthermore, these interactions in TME can be complicated in terms of compositions and cell types, involving multiple ligand-receptor recognitions with numerous interaction strengths and even the average interfacial gap distances[7],

making systematic characterization of direct interactions of tumor cells more problematic.

Compared to imaging-based methods, proximity labeling approaches have been developed to investigate intercellular interactions by *in situ* tagging within the cellular contact environment, integrating advantages of detection, isolation, and downstream analysis[8]. For example, enzyme-based strategies have been successfully applied to capture specific interacting cells, but are limited by genetic manipulation or the complicated synthesis of enzyme conjugates[9-11]. Recently photocatalyst-based approaches have emerged by employing small molecule photocatalysts to generate reactive intermediates, including carbene, singlet oxygen or radical species to drive the proximity labeling process[12-14]. However, due to the inherent chemical activation mechanisms, chemical tuning of these reactive intermediates is usually difficult, hindering the labeling efficiency or adaptation in complex biological environment. Additionally, these methods are hampered by either the generation of damaging chemical species, increasing the risk of altering cell surfaces and fragile biological environments[15,16], or the narrow scope of the labeling substrates, which impeded the unbiased detection of multiple ligand-receptor-based cellular interactions. Therefore, a sensitive, non-invasive, and general platform for interacting cell labeling under physiological relevant conditions is still highly desirable but challenging.

Quinone methides (QMs) are a class of unique efficient Michael acceptors that can be targeted to several widely available nucleophilic residues. It can be facially chemical-modified for tuning the reactivity, and have been widely used in chemical synthesis and chemical biology[17-21]. For the inimitable reactivity and controllable rescue property by protection of its phenol oxygen, QMs have become attractive in combination with bioorthogonal decaging chemistry, which has been developed for on-demand activation of bioactive molecules, allowing gain-of-function manipulations via *in situ* rescue of adaptable caging moieties[22]. In particular, recent bioorthogonal photocatalytic decaging reactions with precise spatiotemporal resolution have shown great potential in widespread applications[23,24], including proximity labeling of intracellular proteins[25]. With the flexibility of the quinone methide reactivity, as well as the bioorthogonality and spatiotemporal controllability of the decaging chemistry, we envisaged that photocatalytic decaging of a suitable quinone methide probe could provide a distinct, universal and efficient chemical approach for diverse cell-cell interaction investigations without damaging the fragile biological components.

Herein, we report the development of a photocatalytic quinone methide decaging-enabled cell-cell interaction labeling strategy, termed CAT-Cell, for profiling the highly diverse intercellular interactions (**Fig. 1a**). The iridium photocatalyst was non-genetically equipped on cells to generate reactive QM intermediates upon visible light irradiation and subsequent labeling targeted diverse protein residues on interacting cells in close proximity. By taking advantage of the chemical tunability of QM probes, our method was sensitive to profile multitype cell-cell interactions to reflect the interacting strengths within various co-culture systems and primary samples. Finally, CAT-Cell allowed cytotoxic cells (including antigen-specific T cells and NK cells) identification in primary samples, emphasizing the critical demand of straightforward, non-disturbing and non-genetic operations under living conditions. Together, CAT-Cell provides a valuable chemical approach for sensitive and universal profiling of multiple cell-cell interactions even without prior knowledge of molecule pairs in diverse living systems.

Results and Discussion

Development and validation of photocatalytic QM-decaging reaction for CCI labeling

We started by developing an intercellular labeling system based on quinone methide chemistry via photocatalytic decaging. In our previous intracellular protein labeling system, high reactive OF2 quinone methide was used for subcellular proteomics profiling[25,26]. However, given the spatially restricted distance and complex intercellular environment, larger labeling radius of quinone methide ensuring sufficient labeling efficiency was needed, which in turn required quinone methide with moderate reactivity resulting from slower quenching rate in aqueous environment. Inspired by the feasible chemical tunability of the quinone methide chemistry, we designed the OF1 probe. Due to the loss of the electron-withdrawing fluorine group comparing with the OF2 counterpart, the quinone methide intermediate of OF1 is expected to be quenched slower because of its less electrophilic reactivity to the nucleophiles including water in the aqueous environment. The photocatalytic decaging of the PAB-protected OF1 probes in aqueous solution were monitored using HPLC first (**Fig. 1b**). Slowly conversion of OF1 into the hydrolyzed product was detected in the presence of both Ir8 (10 mol %) and blue LED irradiation. Nucleophilic addition product was obtained when n-butylamine was added as nucleophile (**Fig. 1b**). Given that labeling reactions on cells usually occur on surface proteins, we next evaluated the protein labeling ability taking BSA as a model protein and the OF2 probe as the reference. As expected, slower labeling rate for OF1 was detected due to its less electrophilic reactivity (**Fig. 1c**).

Next, we aimed to evaluate the capability of intercellular labeling by quinone methide probes, and cell-cell interactions via the CD40-CD40L pair, an important ligand-receptor pair influencing immune activation or suppression[27], was designed and constructed as a model assay (**Fig. 1d**). Two groups of HEK293T cells were transfected with CD40 and CD40L, respectively. Then the CD40L+ cells were equipped with iridium photocatalyst to form the bait cells by treating with NHS-[Ir] (**Supplementary Fig. 1b**). Flow cytometry analysis showed significant biotin signal on the cell surface. We further confirmed membrane protein labeling via western blot analysis, and chose the 100 μM as optimal concentration of NHS-[Ir] for labeling (**Supplementary Fig. 1c, d**). The CD40+ cells were then co-cultured as prey cells and treated with PAB-QM-Bio probes (1 μM), NADH (500 μM), and 5 minutes of blue LED irradiation. After optimization of irradiation, we were delighted to observe significant biotin signals on the CD40+ prey cells via flow cytometry analysis. In contrast, only trace labeling was observed when using CD45+ cells as a non-interacting control (**Fig. 1e, f**), confirming the labeling specificity of which simple colocalization of non-interacting cells with bait cells within the same microenvironment was not adequate to drive labeling process. Additionally, due to the more suitable labeling radius of the less reactive OF1 intermediate, it demonstrated higher labeling efficiency than the OF2 probe (63.9% versus 50.3% labeling ratio) in the *trans*-cell labeling, as expected. These results confirmed the capability of photocatalytic decaging chemistry for specific capturing of the cell-cell interactions, as well as the tunability and flexibility of the labeling probes by decaging strategy.

CAT-Cell is a spatially resolved, modular and targetable CCI labeling strategy

With the established CAT-Cell platform in hand, we sought to explore the versatility of this method for various applications. As a visible light-triggered reaction, the precise photo switch through easily

tunable parameters such as light intensity or duration of CAT-Cell offered a convenient way to achieve spatial specificity when capturing interacting cells in precise regions. As a proof of concept, we cultured HEK293T cells consisting of the CD40-CD40L pair that have been pre-treated and chose a small region of interest (ROI) for photo irradiation, resulting in CAT-Cell-introduced biotinylation (**Fig. 2a**). The labeling efficiency of each well was represented as a "pixel" in the heatmap, in which biotinylation was successfully induced when spatial selectivity to the ROI and cell-cell interaction specificity to the CD40+ cells were simultaneously achieved (**Fig. 2b, c**). The spotless background in the dark region minimized interference from other incoherent zones in complex samples, facilitating the analysis of specific cell-cell interactions.

There are multiple ligand-receptor-based cellular interactions in complex systems, and T cell receptor (TCR)-cognate peptide-major histocompatibility complex (pMHC) recognitions are crucial for orchestrating adaptive immunity, regulating immune surveillance and homeostasis with the help of other adhesion molecules and co-stimulatory/checkpoint receptor-ligand pairs[28-30]. However, it is still challenging to detect specific TCR-pMHC interactions due to the highly diversity and low affinity of TCR repertoires. Thus, we further explored the labeling efficiency and specificity of CAT-Cell in this delicate interaction model. NY-ESO-1 is one of the most immunogenic tumor antigens, widely expressed in various cancers, and is considered an ideal target antigen for tumor immuno-therapy[31,32]. K562 cells expressing HLA-A2:02*01 could present the NY-ESO-$1_{157-165}$ antigen peptide, which can be specifically recognized by JC5 T cells expressing 1G4 TCR but no endogenous TCR. NY-ESO-$1_{157-165}$-3Y (3Y) peptide-primed K562 cells were modified by NHS-[Ir] and co-cultured with 1G4 TCR JC5 cells, followed by CAT-Cell-based biotinylation under blue LED irradiation. Considering the differences in intensity and composition of the CD40-CD40L and TCR-pMHC interactions, we benchmarked the labeling performance of OF1 against OF2 once more. As expected, OF1 showed much more evident labeling efficiency than OF2 (36.3% versus 12.6%), confirming the activity difference between the two probes. Significant biotin signals were detected with the 3Y priming group (36.3%) compared to the no peptide group control (8.9%), indicating the achievement and high specificity of CAT-Cell in a delicate CCI system (**Fig. 2d, e and Supplementary Fig. 2**).

Next, we aimed to investigate the integration of our CAT-Cell with a targeted system that could direct [Ir] localization to a specific cell population. To achieve this, we con-structed a nanobody-photocatalyst conjugate using our previously evolved mono-glycine recognition Sortase A (mgSrtA) and CuAAC click reaction9. This yielded ZHER-$[Ir]_3$ conjugates with three site-specific photocatalysts per ZHER for targeted binding to HER2+ cells (**Fig. 2f and Supplementary Fig. 3a**). ZHER-$[Ir]_3$ was used to bind with HER2+ K562 cells, followed by employment of CAT-Cell (**Fig. 2f**). The HER2+ K562 cells were divided into four groups based on the expression level of HER2, in which the *cis*-labeling ratios were positively correlated with the abundance of HER2 (**Fig. 2g**). We also examined *trans*-labeling in NY-ESO-$1_{157-165}$-3A (3A) peptide-induced CCI system and took the negative control peptide (NC) as a comparison, which binds to HLA-A2:0201 but has no interaction with 1G4 TCR. Significant biotin signals on the HER2+ cells compared to negligible signals on the HER2- cells, as well as the noteworthy biotinylation difference between 3A and NC group, demonstrated the high selectivity and specificity of our targeted strategy in detecting cell type-specific interacting cells (**Fig. 2h, i**). Additionally, we observed similar high specificity and

efficiency of targeted labeling in the CD40-CD40L system (**Supplementary Fig. 3b-d**).

CAT-Cell enables selective and sensitive CCI labeling

Direct physical cell–cell interactions are usually a requirement for initiating and sustaining immune responses, which are influenced by different interaction strengths. It is thus important to characterize the strength of interactions with high sensitivity that may influence molecular responses as well as cell phenotypes and fates. For example, T cells rely on the TCR-pMHC interaction to recognize antigen-presenting cells (APCs). Small differences in this interaction, particularly due to the affinity of the antigen peptide, can result in substantial variations in T cell responses, cytotoxic effects and fate decisions[33-38].

To investigate the ability of the CAT-Cell platform to sensitively distinguish different interaction strengths, we used the TCR-pMHC pair as a model assay to study whether the method could detect interaction differences with varying concentrations and amino acid sequences of the exogenous antigen peptide. A series of altered peptide ligands (APLs) were used to modulate the strength of the interactions between HLA-A2:02*01 K562 cells and 1G4 TCR JC5 cells with NFAT-GFP reporter, which can express GFP after JC5 cells were activated by successful recognition. Thus, we were able to evaluate the interaction strength by biotinylation and take activation level as a reference (**Fig. 3a**). The results showed that the biotin signals significantly increased with increasing antigen concentration, and the biotin+ JC5 cells remained at a low background ratio in the NC group (**Fig. 3b, c**). And the biotin+ population of JC5 cells was highly positively correlated with the GFP expression level, indicating that high-affinity peptide induced high labeling efficiency as well as high T cell activation ratio (**Fig. 3b, c**). We also evaluated the labeling capacity of CAT-Cell by distinguishing NY-ESO-$1_{157-165}$ alternations with single amino acid mutations induced CCIs. The results showed that the ratio of GFP+ and biotin+ population still had a high correlation, and labeling efficiency increased as APLs changed from low affinity to high affinity as expected (**Fig. 3d-f and Supplementary Fig. 4**).

Antigen-specific T cells are usually rare in both tumor tissues and peripheral blood, which made it hard to detect and analysis. The selectivity and sensitivity of CAT-Cell prompted us to investigate its ability to detect antigen-specific T cells in a mixture system at low abundance. We mixed 1G4 TCR JC5 cells and ordinary Jurkat cells at a ratio of 1:99 and carried out intercellular labeling using CAT-Cell (**Fig. 3g**). The results showed that CAT-Cell can specifically label 1G4 TCR JC5 cells even at 1% abundance, while the biotin signal of Jurkat cells still remained at the background level, even though these cells were abundant in the system (**Fig. 3h-j**). Furthermore, the ratio of biotin+ population on 1G4 TCR JC5 cells was still highly correlated with their GFP expression level (**Fig. 3i**). These results demonstrate the high specificity and sensitivity of the CAT-Cell platform. The biotin signal can be used as a chemical marker of CCI to sensitively reflect the strength of ligand-receptor mediated intercellular interactions, avoiding interference from other stimuli.

***Ex Vivo* profiling of interactions between tumor and cytotoxic immune cells**

Considering the reliability of CAT-Cell in detecting antigen-specific JC5 T cells with high accuracy, we assessed its feasibility in primary tissue samples. We chose the model antigen ovalbumin (OVA)-primed MC38 murine colon carcinoma cells to label CD8+ T cells in OT-I transgenic mice

splenocytes. We co-cultured splenocytes with MC38 cells treated with NHS-[Ir] and different antigen peptides, followed by irradiation with blue LED in the presence of the OF1 probe (**Fig. 4a**). We detected an increased biotin signal and T cell activation marker CD69 signal with the $OVA_{257-264}$ treated group compared to the GP_{33-41} group or no peptide control, and the two signals correlated with each other (**Fig. 4b, c and Supplementary Fig. 5a, b**). We also evaluated the labeling efficiency of CAT-Cell to capture other types of immune cells that interact with bait cells stably, such as natural killer (NK) cells[39,40]. We used the MC38-B2M KO cell line which lacks mature MHC-I structure and employed CAT-Cell to profile the difference of interactions between NK cells and target cells (**Fig. 4a**). We observed increased biotinylation on the NK cells co-cultured with MC38-B2M KO rather than normal MC38 cells, confirming enhanced identification and interaction due to the lack of MHC-I (**Fig. 4d and Supplementary Fig. 5c**).

To investigate the selectivity and sensitivity of CAT-Cell, we constructed a mixture system consisting of splenocytes from OT-I mice and C57BL/6 mice and employed CAT-Cell in the mimic system (**Fig. 4a**). We detected increased biotin signals only on the OT-I T cells of the $OVA_{257-264}$ group, as well as activation signals (**Fig. 4e, f and Supplementary Fig. 5d, e**). In contrast, an insignificant labeling background was observed on WT T cells of the $OVA_{257-264}$ group or OT-I T cells of the GP_{33-41} group, likely due to the "non-antigen-specific" interactions existing beyond TCR-pMHC on the cell surface.

Next, we sought to determine whether CAT-Cell could be coupled with antigen-specific T cell detection in tumor samples and further investigated the probability to profile the composition of tumor-infiltrating lymphocytes (TILs) in TME. To verify the ability of CAT-Cell, we employed the MC38-OVA and MC38-B2M KO cell line as models. These two kinds of solid tumors were digested into single-cell suspensions, and MC38 cells with [Ir] pretreatment were respectively loaded with $OVA_{257-264}$ or GP_{33-41} peptide as different bait cells to co-culture with these tumor single-cell suspensions, followed by the interacting cells labeling via CAT-Cell (**Fig. 4g**). To our surprise, only the incubation of $OVA_{257-264}$ primed MC38 and MC38-OVA tumor single-cell suspensions led to the significant biotinylation signals of CD8+ T cells, indicating the primary antigen-specific CD8+ T cells could be detected successfully (**Fig. 4h, i**). By contrast, there was minimal *trans*-labeling of CD8+ T cells when GP_{33-41} primed MC38 co-cultured with MC38-OVA tumor single-cell suspensions, suggesting the specificity of the labeling method of ignoring the influence of simple co-localization. Moreover, only background-level biotinylations were detected in both groups involving MC38-B2M KO tumor single-cell suspensions likely due to the absence of mature MHC complexes, which impacts the antigen presentation as well as the antigen-specific T cells infiltrating. These different labeling results indicate that CAT-Cell is competent to identify antigen-specific T cells with high selectivity and susceptivity in natural complex multicellular environment, and showed the potential to profile unique component difference of TME.

Conclusion

In summary, we have developed a photocatalytic QM-decaging system that enabled intercellular interaction labeling via the bioorthogonal decaging chemistry. Compared to existing photocatalysis-enabled cell capturing methods, CAT-Cell employed distinct QM labeling chemistry, which showed unique advantages. First, the inimitable reactivity of QMs for widespread nucleophilic protein

residues cross multiple cell types made its sensitivity sufficient for detecting the weak and highly dynamic intercellular interactions in an unbiased manner regardless of ligand-receptor involved. Secondly, the chemical tunability of QMs offered a facial approach to improve the labeling efficiency ensuring its extensive application in complex biological scenarios. Additionally, the bioorthogonal QM decaging strategy was more biologically benign and non-invasive, avoiding the potent damaging of prey cells by reactive species previously used for proximity cell labeling such as singlet oxygen, radicals or peroxides. Finally, by coupling the QM chemistry with easily prepared iridium photocatalyst, CAT-Cell is straightforward, non-genetic and with high spatiotemporal resolution, which is highly suitable for primary samples under *ex vivo* or even *in vivo* conditions.

In this work, we designed and developed CAT-Cell to capture multiple ligand-receptor-induced cell-cell interactions and showed its capacity in both cultured cells and primary samples. The sensitivity and selectivity of the labeling method were demonstrated in the TCR-pMHC system and the broad utility was proven by detection of multiple cell types (including HEK293T, antigen-specific T cells and NK cells). By rational design and establishment of quinone methide probes and platforms, we provided a photocatalytic decaging method differing from those doublet-based methods requiring external computational assistant[41] or contact-dependent methods which may have concerns due to the artificial cellular interaction interference[42,43]. It is also complementary to the proximity labeling methods based on specific enzyme or chemical intermediates for intercellular interaction labeling. Considering the chemical tunability of caged QM probes, we expect that there will be more new designs fitting other application scenarios or further improving the labeling efficiency for cell-cell interaction profiling. The design of CAT-Cell is also modular and programmable, permitting the wide adaptability for broad applications. We are currently coupling the CAT-Cell strategy with downstream analyses such as single-cell RNA sequencing, TCR sequencing, and proteomics profiling of tagged cells, which may shed light on the mechanisms of crucial cellular interactions in the immunological process as well as immunotherapy treatment from clinical samples.

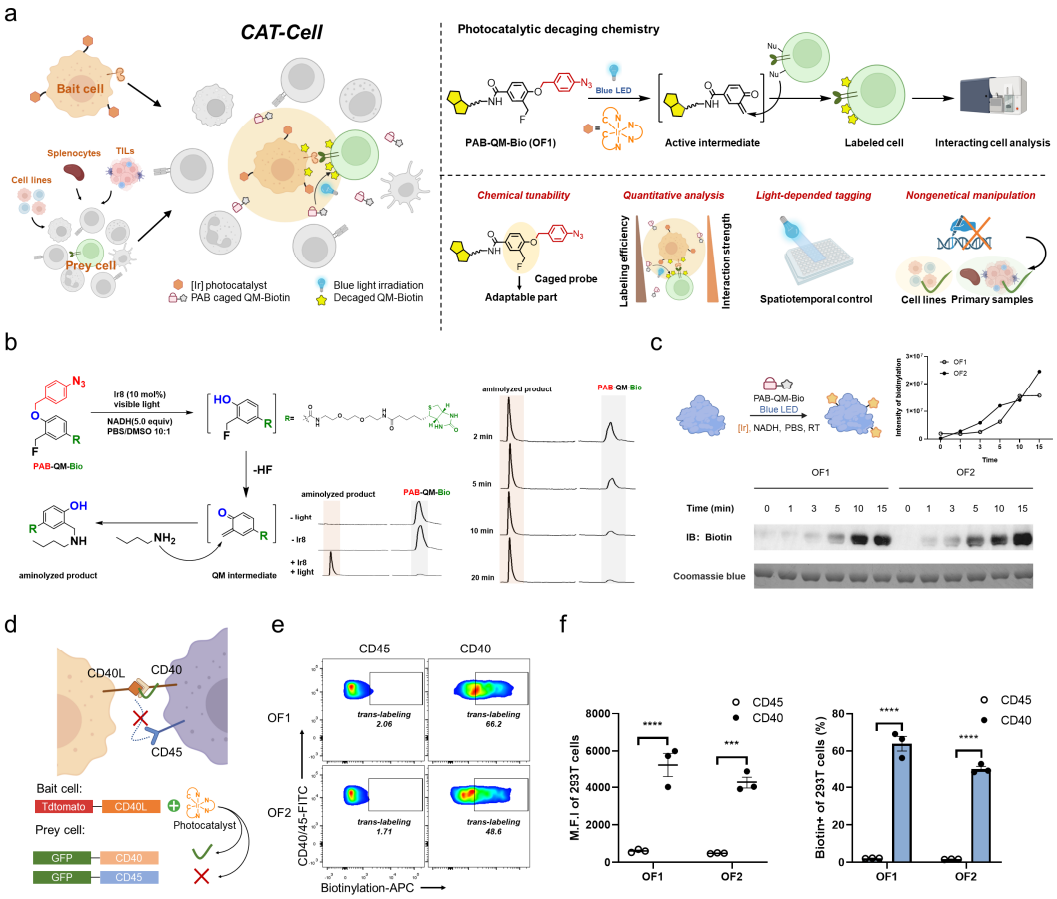

Fig. 1 Design and development of bioorthogonal photocatalytic quinone methide decaging-enabled cell-cell interaction labeling (CAT-Cell).

(a) Schematic illustration of CAT-Cell for labeling cell-cell interactions. Interacting cells can be biotinylated after the reactivation of chemically caged PAB-QM-Bio (OF1) probe by the photocatalytic iridium reagent under mild blue light irradiation. (b) Design of quinone methide-based labeling and HPLC traces of photocatalytic decaging of OF1 in aqueous media. HPLC traces of the photocatalytic decaging of the OF1 probe under blue LED at given time points. Conditions: 0.1 mM OF1, 100 mM butylamine, 0.5 mM NADH, 10 mol % Ir8, in PBS/DMSO (10/1) buffer, irradiated by blue LED (4 mW/cm^2) for 20 min. (c) *In vitro* evaluation of different QM probes by CAT-Cell enabled BSA labeling at given time points. Biotinylated BSA and total BSA were analyzed by immunoblotting and Coomassie blue staining, respectively. (d) Experimental setup to analyze intercellular interactions in transfected HEK293T cells by CAT-Cell. Photocatalytic iridium compound was conjugated on the cell surface via N-hydroxysuccinimide ester–based lysine coupling reaction, allowing bioorthogonal decaging-enabled biotinylation of interacting cells. The CD45+ HEK293T cells were set to be the control group compared to CD40+ cells. (e, f) Flow cytometric analysis (e) and bar graphs (f) showing different biotinylation efficiencies of QM probes. Data are presented as mean ± SEM (n = 3); ns, $p > 0.05$; *$p < 0.05$; **$p < 0.01$; ***$p < 0.001$; ****$p < 0.0001$. Comparisons over groups were analyzed using two-way ANOVA followed by Sidak's multiple comparisons test.

Artworks of (a), (c) and (d) were created with BioRender.com.

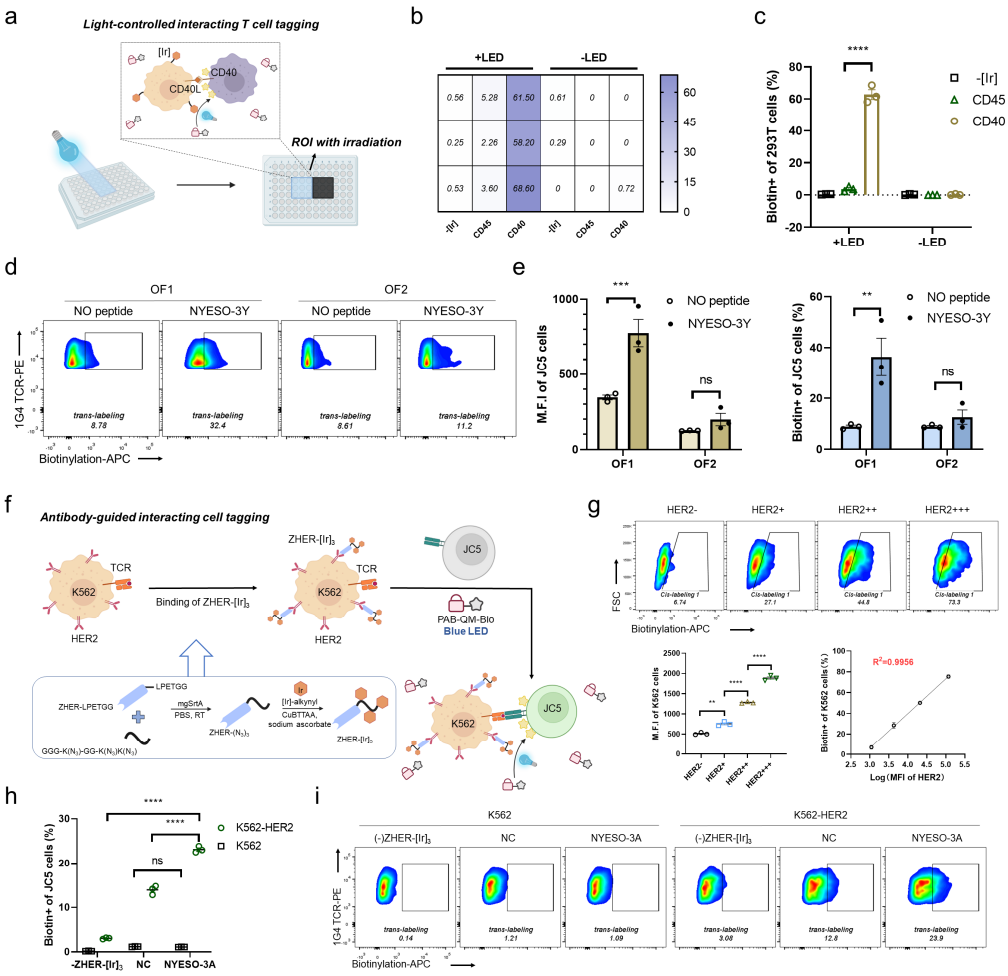

Fig. 2 CAT-Cell enables spatially resolved, modular and targetable labeling of CCIs in various scenarios.

(a) Schematic illustration of CAT-Cell in combination with spatial resolution. Only interacting cells in ROI with irradiation can be biotinylation via CAT-Cell. (b, c) Flow cytometric analysis of biotinylation carried by CAT-Cell in combination with spatial resolution. Heatmaps showing the biotinylation percentage of HEK293T cells with (left) or without (right) blue light irradiation from co-cultures in each well. The tagging percentages were calculated based on FC. (d, e) Flow cytometric analysis showing antigen-specific biotinylation efficiency of different QM probes. HLA-A2:02*01 K562 cells not primed with any antigen peptide ("no peptide" group) was set as negative control. (f) Schematic view of intercellular labeling via CAT-Cell in combination with nanobody-photocatalyst conjugate (ZHER-$[Ir]_3$). [Ir] was conjugated with ZHER via mgSrtA-mediated ligation and click reaction. (g) ZHER-$[Ir]_3$ binding to target cells introduced significant *cis*-labeling under blue light irradiation, and biotinylation efficiency increased along with HER2 expression. R square = 0.9956. (h, i) Flow cytometric analysis of TCR-pMHC interaction-based biotinylation introduced by ZHER-$[Ir]_3$ enabled CAT-Cell. The biotin signals in control groups in which K562 cell without HER2 were all at background level.

Data are presented as mean ± SEM (n = 3); ns, $p > 0.05$; *$p < 0.05$; **$p < 0.01$; ***$p < 0.001$; ****$p < 0.0001$. Comparisons over groups were analyzed using two-way ANOVA followed by Sidak's multiple comparisons test or two-tailed unpaired t test. Artworks of (a) and (f) were created with BioRender.com

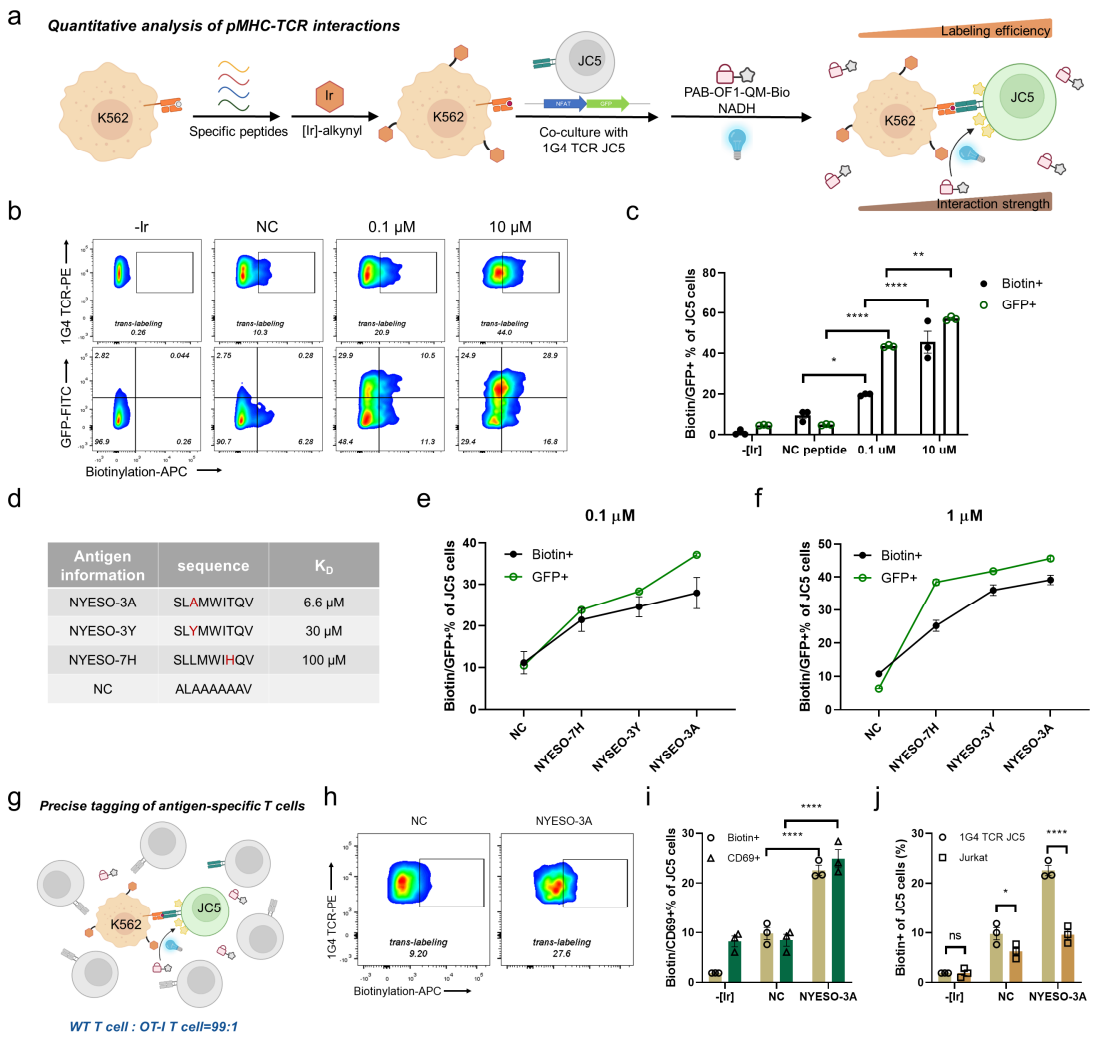

Fig. 3 Characterization of selectivity and sensitivity of CAT-Cell in TCR-pMHC-mediated immune-tumor cell interactions.

(a) Workflow of specific and sensitive labeling of tumor antigen-specific T cells via CAT-Cell. HLA-A2:02*01 K562 cells were loaded with various antigen peptides with varied affinities, followed by the modification of NHS-[Ir] and incubation with the 1G4-TCR JC5 cells which activation can be evaluated by the transfected NFAT-GFP reporter. After biotinylation carried by CAT-Cell, the biotin signals were analyzed by flow cytometry. (b, c) Flow cytometric analysis showing antigen-specific biotinylation and activation degree of 1G4 TCR JC5 cells under different concentration treatment of NY-ESO-$1_{157\text{-}165}$ antigen peptide. NC peptide was a nonspecific antigen peptide which can bind to HLA-A2:02*01 to be used as negative control. (d) Sequences of NY-ESO-$1_{157\text{-}165}$ peptide mutations with varied affinities. (e, f) Flow cytometric analysis showing antigen-specific biotinylation and activation degree of 1G4 TCR JC5 cells with treatments of 0.1 μM (e) or 1 μM (f) antigen peptide mutations with various affinities. The GFP signals were showed by green dots, which correlated with biotin signals (black dots). (g) Schematic illustration of precise tagging of antigen-specific T cells by CAT-Cell in tri-cellular environment. 1G4 TCR JC5 cells were mixed with ordinary Jurkat cells at the ratio of 1:99, and followed by the incubation with bait cells as well as application of CAT-Cell. (h-j) Representative flow cytometric analysis of antigen-specific T cell biotinylation and activation in tri-cellular system. Biotin signals were specifically introduced to 1G4

TCR JC5 cells by CAT-Cell (h-j), with correlated GFP signals (i), while the signals on Jurkat cells were just at back-ground level (j).

Data are presented as mean ± SEM (n = 3); ns, $p > 0.05$; *$p < 0.05$; **$p < 0.01$; ***$p < 0.001$; ****$p < 0.0001$. Comparisons over groups were analyzed using two-way ANOVA followed by Sidak's multiple comparisons test. Artworks of (a) and (g) were created with BioRender.com.

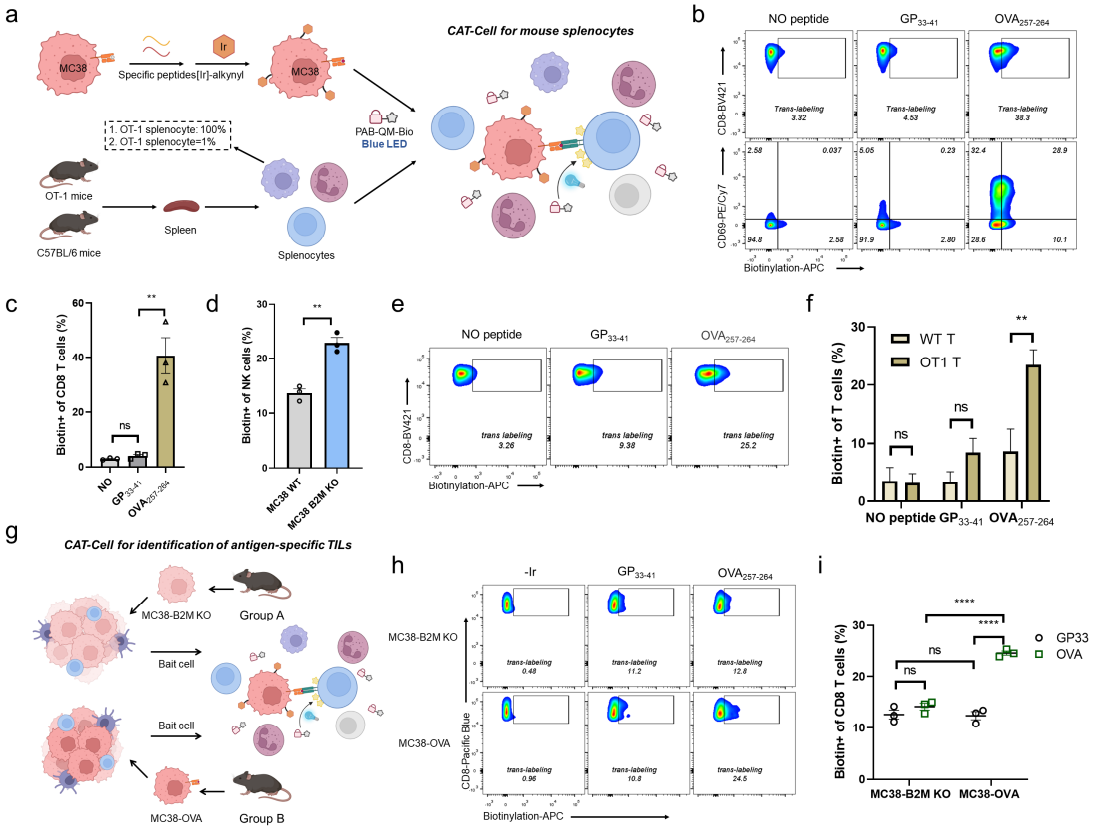

Fig. 4 CAT-Cell enabled *ex vivo* identification of antigen-specific T cells and NK cells.
(a) Experimental setup for CAT-Cell-enabled *ex vivo* identification of antigen-specific T cells and NK cells in the mouse model. OT-I splenocytes were labeled by antigen-primed [Ir]-MC38 or MC38 B2M KO cells after 2 h incubation. OT-I T cells can recognize and interact with MC38 through the specific interaction between transgenic TCRs and $OVA_{257–264}$ peptide-loaded MHC molecules while T cells from C57BL/6 mouse cannot. And the interaction between MC38 B2M KO cells and NK cells can be strengthened due to the loss of mature MHC complex compared with WT MC38 cells. (b, c) Representative flow cytometric analysis of antigen-specific T cell biotinylation in OT-I splenocytes. GP_{33-41} (KAVYNFATM) was a nonspecific antigen peptide from the lymphocytic choriomeningitis virus (LCMV). The biotin signals in $OVA_{257–264}$ groups correlated with GFP signals in (b). (d) Flow cytometric analysis of primary NK cells interacting with different MC38 cells. The loss of mature MHC structure made MC38 B2M KO cell easier to active NK cells so that the interaction can be enhanced as well as the biotin signals. (e, f) Characterization of sensitivity and specificity of CAT-Cell in multicellular environment. Splenocytes from OT-I mouse and C57BL/6 mouse were mixed up to mimic a complex multicellular environment, which followed by interacting cell profiling via CAT-Cell. Flow cytometric analysis of antigen-specific T cell biotinylation of splenocytes. Only the OT-I T cells from OT-I mouse can be biotinylated specifically. (g) Schematic illustration of antigen-specific TILs identification via CAT-Cell in MC38 tumor models. The C57BL/6 mice were planted with MC38 or MC38 B2M KO cells separately and harvested subcutaneous solid tumors were digested into single-cell suspensions. After tumor-T interaction, CAT-Cell-induced labeling was carried out, and the biotin signal was analyzed by FC. (h, i) Representative flow cytometric analysis of antigen-specific biotinylation of TILs in the mouse MC38 tumor model.

Data are presented as mean ± SEM (n = 3); ns, $p > 0.05$; *$p < 0.05$; **$p < 0.01$; ***$p < 0.001$; ****$p < 0.0001$. Comparisons over groups were analyzed using two-way ANOVA followed by Sidak's multiple comparisons test or two-tailed unpaired t test. Artworks of (a) and (g) were created with BioRender.com.

Associated content

Supplementary information

Materials, protocols and data characterizations for all biological and chemical experiments are described in detail in the Supplementary information.

Author information

P.R.C., X.F. and S.L. conceived the study. X.F. and P.R.C. supervised the project. Y.Z., F.G., S.Q. and N.Z. performed the experiments and analyzed the data. S.L. helped with data analysis, project discussion and manuscript preparation. Y.Z., X.F. and P.R.C. wrote the paper with input from all authors.

Notes

The authors declare no competing interests.

Acknowledgment

We acknowledge funding from the National Natural Science Foundation of China (22222701, 22077004, 92253301, 21937001, 22137001), the Ministry of Science and Technology (2019YFA0904201, 2022YFA1304700, 2022YFE0114900), Beijing Natural Science Foundation (Z200010) and Li Ge-Zhao Ning Life Science Junior Research Fellowship.

References

1 Bonnans, C., Chou, J. & Werb, Z. Remodelling the extracellular matrix in development and disease. *Nat. Rev. Mol. Cell Biol.* **15**, 786-801 (2014).

2 Armingol, E., Officer, A., Harismendy, O. & Lewis, N. E. Deciphering cell–cell interactions and communication from gene expression. *Nat. Rev. Genet.* **22**, 71-88 (2020).

3 Demaria, O. et al. Harnessing innate immunity in cancer therapy. *Nature* **574**, 45-56 (2019).

4 Binnewies, M. et al. Understanding the tumor immune microenvironment (TIME) for effective therapy. *Nat. Med.* **24**, 541-550 (2018).

5 Huang, A. C. & Zappasodi, R. A decade of checkpoint blockade immunotherapy in melanoma: understanding the molecular basis for immune sensitivity and resistance. *Nat. Immunol.* **23**, 660-670 (2022).

6 Fridman, W. H., Zitvogel, L., Sautès–Fridman, C. & Kroemer, G. The immune contexture in cancer prognosis and treatment. *Nat. Rev. Clin. Oncol.* **14**, 717-734 (2017).

7 Belardi, B., Son, S., Felce, J. H., Dustin, M. L. & Fletcher, D. A. Cell–cell interfaces as specialized compartments directing cell function. *Nat. Rev. Mol. Cell Biol.* **21**, 750-764 (2020).

8 Bechtel, T. J., Reyes-Robles, T., Fadeyi, O. O. & Oslund, R. C. Strategies for monitoring cell–cell interactions. *Nat. Chem. Biol.* **17**, 641-652 (2021).

9 Pasqual, G. et al. Monitoring T cell-dendritic cell interactions in vivo by intercellular enzymatic labelling. *Nature* **553**, 496-500 (2018).

10 Ge, Y. et al. Enzyme-mediated intercellular proximity labeling for detecting cell-cell interactions. *J. Am. Chem. Soc.* **141**, 1833-1837 (2019).

11 Liu, Z. L. et al. Detecting tumor antigen-specific T cells via interaction-dependent fucosyl-biotinylation. *Cell* **183**, 1117-1133 (2020).

12 Oslund, R. C. et al. Detection of cell–cell interactions via photocatalytic cell tagging. *Nat. Chem.*

Biol. **18**, 850-858 (2022).

13 Liu, H. et al. Antigen-specific T cell detection via photocatalytic proximity cell labeling (PhoXCELL). *J. Am. Chem. Soc.* **144**, 5517-5526 (2022).

14 Geri, J. B. et al. Microenvironment mapping via Dexter energy transfer on immune cells. *Science* **367**, 1091-1097 (2020).

15 Jemas, A. et al. Catalytic activation of bioorthogonal chemistry with light (CABL) enables rapid, spatiotemporally controlled labeling and no-sash, subcellular 3D-patterning in live cells using long wavelength light. *J. Am. Chem. Soc.* **144**, 1647-1662 (2022).

16 Davies, M. J. Singlet oxygen-mediated damage to proteins and its consequences. *Biochem. Biophys. Res. Commun.* **305**, 761-770 (2003).

17 Bai, W.-J. et al. The domestication of ortho-quinone methides. *Acc. Chem. Res.* **47**, 3655-3664 (2014).

18 Toteva, M. M. & Richard, J. P. The generation and reactions of quinone methides. *Adv. Phys. Org. Chem.* **45**, 39-91 (2011).

19 Parra, A. & Tortosa, M. para-Quinone methide: a new player in asymmetric catalysis. *ChemCatChem* **7**, 1524-1526 (2015).

20 Gnaim, S. & Shabat, D. Quinone-methide species, a gateway to functional molecular systems: from self-immolative dendrimers to long-wavelength fluorescent dyes. *Acc. Chem. Res.* **47**, 2970-2984 (2014).

21 Liu, J. et al. Photocaged quinone methide crosslinkers for light‐controlled chemical crosslinking of protein‐protein and protein‐DNA complexes. *Angew. Chem. Int. Ed.* **58**, 18839-18843 (2019).

22 Wang, J., Wang, X., Fan, X. & Chen, P. R. Unleashing the power of bond cleavage chemistry in living systems. *ACS Cent. Sci.* **7**, 929-943 (2021).

23 Chen, Y., Kamlet, A. S., Steinman, J. B. & Liu, D. R. A biomolecule-compatible visible-light-induced azide reduction from a DNA-encoded reaction-discovery system. *Nat. Chem.* **3**, 146-153 (2011).

24 Angerani, S. & Winssinger, N. Visible light photoredox catalysis using Ruthenium complexes in chemical biology. *Chem. Eur. J.* **25**, 6661-6672 (2019).

25 Huang, Z. et al. Bioorthogonal photocatalytic decaging-enabled mitochondrial proteomics. *J. Am. Chem. Soc.* **143**, 18714-18720 (2021).

26 Liu, Z. et al. Spatially resolved cell tagging and surfaceome labeling via targeted photocatalytic decaging. *Chem* **8**, 2179-2191 (2022).

27 Chand Dakal, T. et al. Mechanistic basis of co-stimulatory CD40-CD40L ligation mediated regulation of immune responses in cancer and autoimmune disorders. *Immunobiology* **225**, 151899 (2020).

28 Dustin, M. L. The Immunological Synapse. *Cancer Immunol. Res.* **2**, 1023-1033 (2014).

29 Yokosuka, T. & Saito, T. The immunological synapse, TCR microclusters, and T cell activation. *Curr. Top. Microbiol. Immunol.* **340**, 81–107 (2010).

30 Huppa, J. B. & Davis, M. M. T-cell-antigen recognition and the immunological synapse. *Nat. Rev. Immunol.* **3**, 973-983 (2003).

31 Millar, D. G. et al. Antibody-mediated delivery of viral epitopes to tumors harnesses CMV-specific T cells for cancer therapy. *Nat. Biotechnol.* **38**, 420-425 (2020).

32 Thomas, R. et al. NY-ESO-1 based immunotherapy of cancer: current perspectives. *Front.*

Immunol. **9**, 947 (2018).

33 Lever, M. et al. Architecture of a minimal signaling pathway explains the T-cell response to a 1 million-fold variation in antigen affinity and dose. *Proc. Natl. Acad. Sci. USA* **113**, 6630-6638 (2016).

34 Voisinne, G. et al. Kinetic proofreading through the multi-step activation of the ZAP70 kinase underlies early T cell ligand discrimination. *Nat. Immunol.* **23**, 1355-1364 (2022).

35 Voisinne, G. et al. Quantitative interactomics in primary T cells unveils TCR signal diversification extent and dynamics. *Nat. Immunol.* **20**, 1530-1541 (2019).

36 Howden, A. J. M. et al. Quantitative analysis of T cell proteomes and environmental sensors during T cell differentiation. *Nat. Immunol.* **20**, 1542-1554 (2019).

37 Zhong, S. et al. T-cell receptor affinity and avidity defines antitumor response and autoimmunity in T-cell immunotherapy. *Proc. Natl. Acad. Sci. USA* **110**, 6973-6978 (2013).

38 Skokos, D. et al. Peptide-MHC potency governs dynamic interactions between T cells and dendritic cells in lymph nodes. *Nat. Immunol.* **8**, 835-844 (2007).

39 Myers, J. A. & Miller, J. S. Exploring the NK cell platform for cancer immunotherapy. *Nat. Rev. Clin. Oncol.* **18**, 85-100 (2021).

40 Morvan, M. G. & Lanier, L. L. NK cells and cancer: you can teach innate cells new tricks. *Nat. Rev. Cancer* **16**, 7-19 (2016).

41 Giladi, A. et al. Dissecting cellular crosstalk by sequencing physically interacting cells. *Nat. Biotechnol.* **38**, 629-637 (2020).

42 Zhang, S. et al. Monitoring of cell-cell communication and contact history in mammals. *Science* **378**, eabo5503 (2022).

43 Stevens, A. J. et al. Programming multicellular assembly with synthetic cell adhesion molecules. *Nature* **614**, 144-152 (2023).